PAPER

Cite this: *RSC Adv.*, 2017, **7**, 2869

A facile synthesis of Cu–Ni bimetallic nanoparticle supported organo functionalized graphene oxide as a catalyst for selective hydrogenation of *p*-nitrophenol and cinnamaldehyde†

Surjyakanta Rana and Sreekantha B. Jonnalagadda*

We report a facile and environmentally friendly protocol for the synthesis of novel mono-dispersed Cu and Ni bimetallic alloy particles supported on fibrous anime functionalized graphene oxide (GO). In this protocol, we used the organic amine group to increase the binding capacity of supported metal particles. First GO was covalently functionalized by organic amine [*N*-(2 amino ethyl)-3-amino propyl trimethoxy silane *i.e.*, (AAPTMS)] to form AAPTMS–GO and then metal ions were loaded on the surface of the AAPTMS–GO material. The metal particles supported on AAPTMS functionalized graphene oxide were named as Ni–AAPTMS–GO, Cu–AAPTMS–GO and Cu–Ni–AAPTMS–GO to reflect the metals loaded, and all were fully characterized by various techniques including XRD, SEM, FTIR, Raman spectra, TEM and HRTEM analysis. The 5% loaded with a 1 : 1 ratio of Cu : Ni of Cu(0)–Ni(0)–AAPTMS–GO showed superb efficiency in conversion of *p*-nitrophenol to *p*-aminophenol with 100% conversion and selectivity. Hydrogenation of cinnamaldehyde with the same catalyst gave 85% conversion and 59.8% selectivity towards cinnamal alcohol (COL) at 80 °C. The catalyst also showed good stability in recycling tests.

1 Introduction

Single metal nano catalysts, such as Pd, Pt and Ru are known to be effective catalysts for reduction of aromatic compounds.[1] However, these single metal nanoparticles are less selective and get quickly deactivated.[2,3] Due to the unique properties at the nanoscale, the bimetallic nanomaterials[4,5] have recorded versatile applications as catalysts[6,7] and many other fields of chemical industry.[8] The excellent synergy between their constituent elements, in addition to size effects are the main reasons for the enhanced catalytic activity by bimetallic nano-particles. Pd–Au nano bimetallic materials, for example exhibit better catalytic activity than their monometallic ones, towards the oxidation of CO, alcohols and C–H bonds, and in the synthesis of H_2O_2 from H_2 and O_2.[9–14]

Primary drawback associated with unsupported catalysis is that metallic catalysts cannot be reusable for several catalytic runs. Whereas with supported heterogeneous catalysts, allow easy separation and reusability, which is an attractive advantage. Although some agglomeration of metal nanoparticles during catalytic runs is inevitable, a right choice of support will minimize such processes. The supports containing organic groups can greatly influence the activity and selectivity of the catalyst material. Due to the nontoxicity and high sorption capacities,[15–18] carbon based nanomaterials have been widely used as inorganic support for catalyst materials. In material science, graphene oxides enjoy prime position among the other carbon based materials, due to their honey comb like structure and high surface area.[19,20]

Transition metal salts like Cu and Ni are less-expensive and readily available, relative to the most of noble metal salts, which are normally used as catalysts. Therefore, in the current study, we have constructed low-cost Cu–Ni bimetallic nano particles grafted on amine functionalized graphene oxide surface. The amine functionalized graphene oxide as support material possess high surface area, which enhances the catalytic activity as well as dispersion capacity. The functionalized amine with external binding capacity will provide additional active sites and also increase its reusability.

Nitro substituted hydrocarbons are generally toxic by nature and hard to be degraded in the environment.[21] In addition, the conversion of aromatic nitro-compounds to aromatic amino compounds obeys with the demands of green chemistry. Further, hydrogenation of unsaturated aldehyde to alcohol with heterogeneous catalytic processes is always a challenge, since the hydrogenation of the C=O bond, while keeping the C=C intact is not thermodynamically favourable. Thus, the

School of Chemistry & Physics, College of Agriculture, Engineering & Science, University of KwaZulu-Natal, Durban, South Africa. E-mail: jonnalagaddas@ukzn.ac.za; Fax: +27 31 260 3091; Tel: +27 31 260 7325 ext. 3090

† Electronic supplementary information (ESI) available. See DOI: 10.1039/c6ra26443c

hydrogenation is of supreme significance in fine chemical synthesis and many efforts have been made to design appropriate solid catalysts. Prakash *et al.* have reported that Ni–Au/TiO$_2$ and Ni–Ag/TiO$_2$ gave better activity towards hydrogenation of unsaturated aldehyde compared to their single mono metallic like Ni/TiO$_2$.[22] Lin *et al.*, have also reported that Ir–Ni/TiO$_2$ catalyst showed higher activity and selectivity in hydrogenation of unsaturated aldehydes compared to heterogeneous monometallic catalysts.[23]

In this study we developed a novel catalyst material, Cu–Ni bimetallic functionalised graphene oxide nanocomposite and investigated its activity on two organic transformations. The efficacy of the different loading of Cu and Ni on the support for selective reduction of *p*-nitrophenol as well as hydrogenation of cinnamaldehyde were examined and role of temperature and solvents on the reactions were assessed.

2 Experimental

2.1 Preparation of GO

0.5 g of graphite powder, 0.5 g of NaNO$_3$ and con. H$_2$SO$_4$ (23 ml) in a beaker and constant stirring in ice bath for 2 h. 3 g of KMnO$_4$ was added slowly and stirring continued for 70 min. Then, distilled water (50 ml) was added to the mixture. The reaction mixture was stirred at 35 °C for 1 h and 98 °C for another 20 min. Then, (30%) H$_2$O$_2$ was added to the mixture and stirred for 1 h till the colour of the mixture turned dark brown to yellow. Water (50 ml) was added to the mixture and

stirred for 1 h. Then, the final mixture was sonicated for 30 min. The sonicated product was centrifuged with 10% HCl and filtered with DD water several times. Then, the final solid material was dried at 40 °C in a vacuum oven for overnight to acquire graphene oxide (GO).
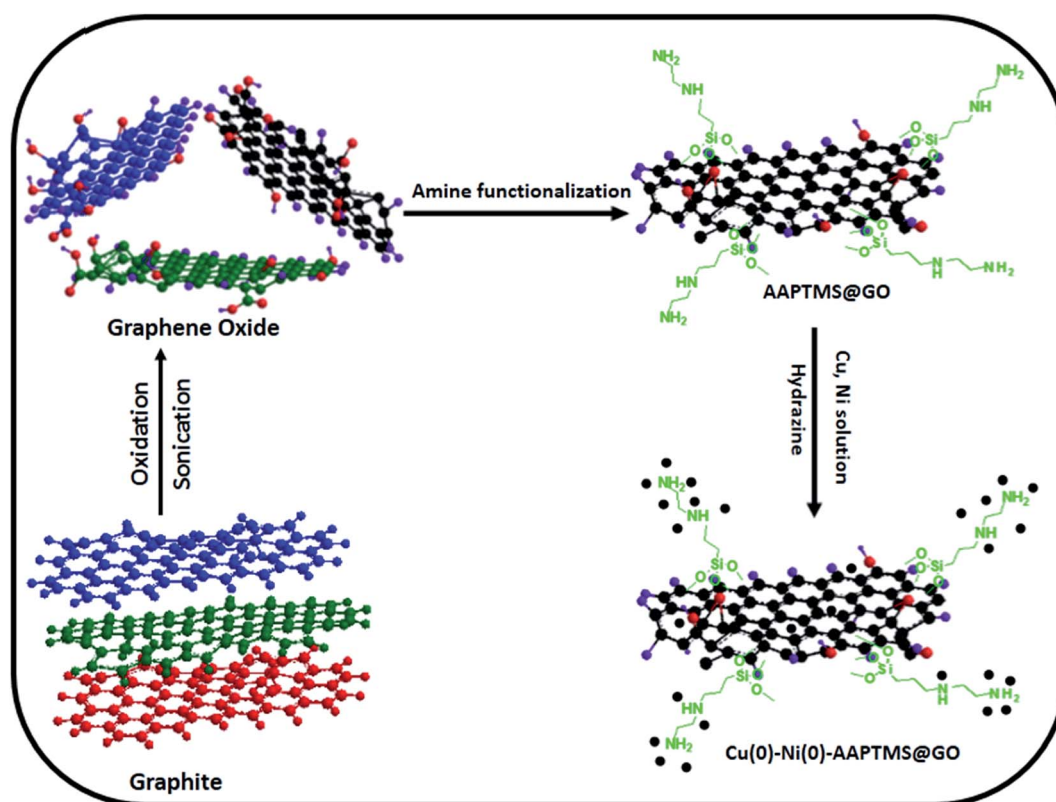
2.2 AAPTMS@GO

Graphene oxide (1 g) was dissolved in 50 ml ethanol solution in a conical flask and sonicated for 1 h. 1.68 mmol of AAPTMS [(3-(2-aminoethylamino) propyl] trimethoxysilane) was drop wise added to the mixture and sonicated for 1 h. Then, the mixture was centrifuged and the product was dried at 40 °C in a vacuum oven for overnight to get AAPTMS@GO.

2.3 Cu–Ni–AAPTMS@GO

Bimetallic Cu–Ni composites were prepared by incipient wetness impregnation method. The copper nitrate and nickel nitrate were mixed to get the subsequent metallic (Cu : Ni) molar ratios such as 1 : 0, 0 : 1, 1 : 1, 1 : 2, and 2 : 1. The metallic solutions were added to 4.75 g of amine functional GO solution. The liquid phase was removed by a 4 h treatment at 70 °C in a rotary evaporator and then dried in vacuum overnight at 100 °C.

Similar method was used for preparation of Cu–Ni bimetallic nanoparticles by using hydrazine. To the Cu and Ni containing solution of functionalized GO, 0.2 M hydrazine solution was added under stirring. Then the suspension was vigorously

Scheme 1 Preparation of the Cu(0)−Ni(0)−AAPTMS@GO catalyst.

stirred at RT for 6 h. The suspension was washed with acetone and preserved toluene. Then, the final solid product was vacuum dried at 100 °C for overnight (Scheme 1).

2.4 Equipment and methods

The X-ray diffraction study was performed on a Bruker D8 Advance instrument with CuKα as a radiation source. The transmitted electron microscopy images were observed on a Jeol JEM-1010 electron microscope with iTEM software. Jeol JEM 2100 Electron Microscope was used for capturing high resolution of TEM images. The JEOL JSM-6100 microscope was used for both scanning electron microscopy and EDX measurements. PerkinElmer spectrum 100 series with universal ATR accessory used for Fourier transmission infrared spectrometer (FTIR). The weight percentages of Cu and Ni in the bimetallic catalyst were determined by using inductively coupled plasma-optical emission spectroscopy (ICP-OES) (Perkin Elmer Optima 5300 DV). UV-visible spectra were recorded with high resolution spectrometer (HR2000+). Raman spectra were observed on a Perkin Elmer 1200 Fourier Transform Infrared and on a DeltaNu advantage 532™ Raman Spectrometer. The electronic structure aspects of the samples were investigated using KRATOS apparatus with Mg, Al, and Cu Kα as X-ray sources by XPS. The illustrative products were analyzed by ^{1}H NMR (Bruker, 400 MHz, [d$_6$] DMSO) ^{13}C NMR (Bruker, 400 MHz, [d$_6$] DMSO) and FTIR spectroscopies (PerkinElmer).

2.5 Catalytic reaction of PNP to PAP

NaBH$_4$ (60 mg) and 5.0 mM of *p*-nitrophenol (30 ml) were taken in a round bottom flask and stirred randomly to homogenize the solution. 3.0 mg of catalyst was added after getting the yellow colour. The change of *p*-nitrophenolate to *p*-amino-phenol was observed by gradual discoloration. Aliquots of the mixture were removed at 4 min intervals and the absorption spectrum the reaction mixture was recorded using a UV-Vis spectrometer. While absorbance at 400 nm reflecting concentration of nitrophenolate species decreased, the value of absorbance at 300 nm steadily increased indicating the formation of *p*-aminophenol. After the completion of reaction, the solid catalyst was retrieved with centrifugation and washed with DD water after each catalytic cycle. The reaction products were also characterized by comparing the ^{1}H NMR, ^{13}C NMR and FTIR data with authentic samples.

2.5.1 Reduction of nitro aromatic compound PAP characterization data. The following product was identified and confirmed by comparison with previously reported spectroscopic data, *p*-aminophenol: ^{1}H NMR δ_H (400 MHz, DMSO [d$_6$]): 4.35 (2H), 6.39–6.47 (4H), 8.32 (1H). ^{13}C NMR δ_C (400 MHz, DMSO [d$_6$]): 115.22, 115.48, 140.58, 148.16 ppm. FTIR: $\nu^- =$ 1614, 845, 1509, 1473, 1385, 3339 cm^{-1}.

2.6 General procedure for hydrogenation of cinnamaldehyde

150 mg of catalyst, 1.2 g of cinnamaldehyde and 16 ml of methanol were taking in a round three necked volumetric flask fitted with water circulating condenser, after purging first with

nitrogen. Then the reaction was stirred with continuous flow of hydrogen. The reactions were carried out at 80–120 °C for 1 h. The resulting mixture was analysed by GC. The catalyst was recovered by the simple centrifugation and washed with D.D. water.

3 Results and discussion

3.1 Surface characterization

The X-ray diffraction patterns of AAPTMS@GO (a), Ni–AAPTMS@GO (b), Cu–AAPTMS@GO (c), (1 : 1) Cu–Ni–AAPTMS@GO (d), (1 : 1) Cu(0)–Ni(0)–AAPTMS@GO (e), (1 : 2) Cu(0)–Ni(0)–AAPTMS@GO (f), and (2 : 1) Cu(0)–Ni(0)–AAPTMS@GO (g) are shown in Fig. 1. According to the literature,[24] graphite shows a diffraction peak at $2\theta = 26.18°$ ($d = 0.34$ nm) resembles to the normal basal spacing (002) of the graphite plane, but the peak vanishes when it is converted to graphene oxide (GO). In GO, the characteristic diffraction peak of (002) plane is observed approximately at 10.651° and (100) plane corresponding to 2θ at 42.91° due to the hexagonal structure of carbon.[25–28] The interlayer spacing of GO increases from 0.34 nm to 0.7964 nm, during the oxidation process of graphite to GO, which may be due to the formation of oxygen-containing functional groups on the graphene oxide surfaces. In the X-ray diffraction pattern of amine functionalized graphene oxide in Fig. 1(a), the (002) plane has shifted towards a lower angle, *i.e.*, $2\theta \approx 9.56$. This is attributed to the stitching of individual GO layers by the amine functional groups.[29] The XRD illustrations, after modification of the functionalized GO surface with 5 wt% of (1 : 1) ratio of bimetal (Cu and Ni) [Fig. 1(b)–(d)], display various forms of the metals, *i.e.*, metal oxide, metal hydroxide *etc.* When, hydrazine was added, it reduced all those forms to metallic nano particles in (1 : 1) Cu(0)–Ni(0)–AAPTMS@GO (Fig. 1(e)). In Fig. 1(e), the existence of sharp and strong diffraction peaks at 2θ, 43.51°, 50.81° and 74.81° respectively
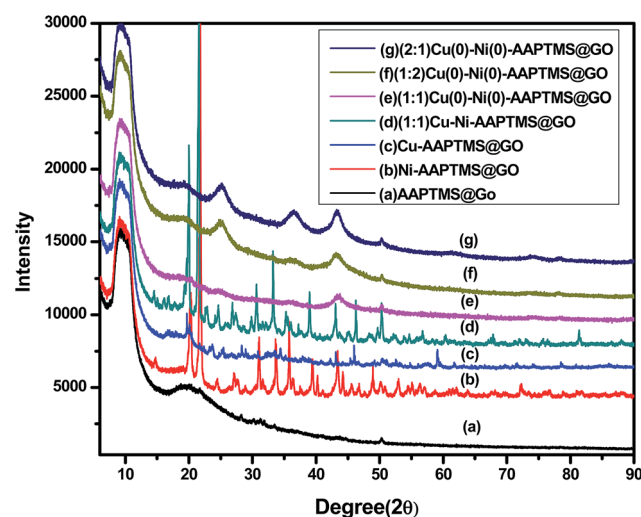

Fig. 1 X-ray diffraction patterns of AAPTMS@GO (a), Ni–AAPTMS@GO (b), Cu–AAPTMS@GO (c), (1 : 1) Cu–Ni–AAPTMS@GO (d), (1 : 1) Cu(0)–Ni(0)–AAPTMS@GO (e), (1 : 2) Cu(0)–Ni(0)–AAPTMS@GO (f), and (2 : 1) Cu(0)–Ni(0)–AAPTMS@GO (g).

Fig. 2 XPS profiles of Cu and Ni 2p level for (1 : 1) Cu(0)–Ni(0)–AAPTMS@GO samples.

correspond to (111), (200) and (220) planes, indicating the formation of a pure cubic bimetallic well dispersed Cu–Ni alloy nanoparticles.[30] This was also confirmed from HRTEM. With the (1 : 2) and (2 : 1) ratio of Cu(0)–Ni(0)–AAPTMS@GO materials [Fig. 1(f) and (g)], in addition to pure metal alloy, some metal oxides were also found. The (1 : 1) Cu(0)–Ni(0)–AAPTMS@GO in Fig. 1(e), confirms the formation of pure metallic nano alloy with uniform distribution over the organo-functionalized graphene oxide sheets.

The FT-IR spectra (4000–400) of (a) AAPTMS@GO, (b) Ni–AAPTMS@GO, (c) Cu–AAPTMS@GO, (d) (1 : 1) Cu–Ni–AAPTMS@GO, (e) (1 : 1) Cu(0)–Ni(0)–AAPTMS@GO, (f) (1 : 2) Cu(0)–Ni(0)–AAPTMS@GO, and (g) (2 : 1) Cu(0)–Ni(0)–AAPTMS@GO are shown in ESI Fig. S1.† All the samples showed peaks at 3400 cm^{-1} and 1740 cm^{-1} due to O–H stretching, C=O stretching of –COOH. The peaks at 1385 cm^{-1} and 1100 cm^{-1} also correspond to O–H vibration of C–OH groups and epoxy group vibration.[31] The covalent functionalization of organic amine proceeds through two steps. In the first step, trialkoxy groups of silane generate –Si–OH groups by hydrolysis. Then the second step, the reaction between –Si–OH group of organo silane and –C–OH group of graphene oxide, covalently linked to the graphene surface through –Si–O–C– bond. In the FTIR spectra, the peak at 686 cm^{-1} is due to stretching vibrations of Si–O–C.[32] The peaks at 3371 cm^{-1} and 1638 cm^{-1} corresponding to N–H stretching and NH$_2$ bending mode of free NH$_2$ groups due to the organic amine modification. These peaks give direct evidence to the successful silylation of the GO materials.

The Raman spectra of AAPTMS@GO (a), Cu–AAPTMS@GO (b), Ni–AAPTMS@GO (c), (1 : 1) Cu–Ni–AAPTMS@GO (d) and (1 : 1) Cu(0)–Ni(0)–AAPTMS@GO (e) are shown in ESI Fig. S2.† All the five samples showed similar characteristic D and G bands. In GO, the band at 1350 cm^{-1} corresponds to disorder in the sp^2-hybridized carbon atoms in graphene oxide sheets from D-band, and 1590 cm^{-1} represents the σ-sp^2 bonded C-atoms from G band of Raman spectra.[31] After metal modification, the both D and G-band moved nearer to higher wave number, which may be due to the progressively increased compressive local stress caused by molecule intercalation as shown in ESI Fig. S2(a–e).†

X-ray photo electron spectroscopy give the information about the binding energy of Cu 2p and Ni 2p in (1 : 1) Cu(0)–Ni(0)–AAPTMS@GO catalyst in Fig. 2. The binding energy of Cu 2p$_{3/2}$
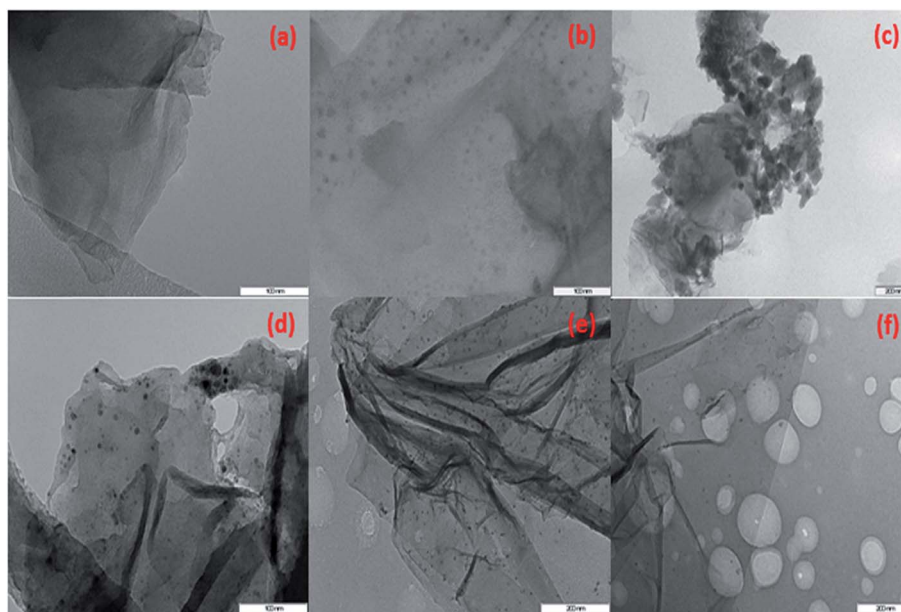

Fig. 3 TEM image of (a) AAPTMS@GO (scale bar = 100 nm) (b) Cu–AAPTMS@GO (scale bar = 100 nm) (c) (1 : 1) Cu–Ni–AAPTMS@GO (scale bar = 200 nm) (d) (1 : 1) Cu(0)–Ni(0)–AAPTMS@GO (scale bar = 100 nm) (e) (1 : 2) Cu(0)–Ni(0)–AAPTMS@GO (scale bar = 200 nm) and (f) (2 : 1) Cu(0)–Ni(0)–AAPTMS@GO (scale bar = 200 nm).

and Cu $2p_{1/2}$ are 932.3 eV and 952.12 eV respectively. The binding energy of Cu $2p_{3/2}$ was ∼0.5 eV lower than that in the metallic state of Cu. The binding energy of Ni $2p_{3/2}$ and Ni $2p_{1/2}$ are 853.5 eV and 873.3 eV respectively, which was ∼0.5 eV higher than that in the metallic state of Ni catalyst.[33] The shifting of binding energies of Cu $2p_{3/2}$ and Ni $2p_{3/2}$ confirm the formation of alloy nanoparticles between Cu and Ni and also interaction between metallic alloy and support surface.

TEM images of AAPTMS@GO (a), Cu–AAPTMS@GO (b), (1 : 1) Cu–Ni–AAPTMS@GO (c), (1 : 1) Cu(0)–Ni(0)–AAPTMS@GO (d), (1 : 2) Cu(0)–Ni(0)–AAPTMS@GO (e) and (2 : 1) Cu(0)–Ni(0)–AAPTMS@GO (f) samples, facilitate to examine the morphologies of the synthesized materials are shown in Fig. 3. The pure graphene oxide is composed of very thin sheets.[28] After functionalization silane creates defects in the graphene oxide sheets, this morphology changes due to presence of organic solvents. The solvent appears to soften the severe attack of organic amine groups on GO surface and hinders breaking down of big sheets to smaller ones as shown in Fig. 3(a). Fig. 3(b) displays the only single metal particles, but in Fig. 3(c) displays the different phase of complex morphology of both bimetallic particles are formed, which is concurrent with the XRD study. After reduction of Cu and Ni metals by hydrazine in the Fig. 3(d)–(f), it can be seen that the well mono-dispersed Cu–Ni bimetallic nano particles are distributed on the functionalized graphene oxide sheets.

The SEM images of AAPTMS@GO (a), Cu–AAPTMS@GO (b), (1 : 1) Cu–Ni–AAPTMS@GO (c), (1 : 1) Cu(0)–Ni(0)–AAPTMS@GO (d), (1 : 2) Cu(0)–Ni(0)–AAPTMS@GO (e) and (2 : 1) Cu(0)–Ni(0)–AAPTMS@GO (f) are shown in Fig. 4. From these images, the broken smaller sheets observed are formed after functionalization due to the interaction between silane and functional group of graphene oxide surface in the presence of organic solvent. The surface morphology of the materials was not changed after reduction of metals with hydrazine.

EDX spectroscopy gives the evidence on the type of element existing in the specific area. The SEM-EDX mapping of (1 : 1) Cu(0)–Ni(0)–AAPTMS@GO sample is presented in the Fig. 5. From these images, the presence of silicon, carbon, nitrogen, oxygen, Cu and Ni in this material can be seen. Another most vital and valuable ability of the EDX technique is X-ray mapping of elements. The positions of particular elements emitting specific X-rays within a scrutiny field are indicated by unique colors. The maps of distribution of elements like Si, C, N, O, Cu and Ni are exposed individually and overlapped with the original image as shown in the Fig. 5. The elemental mapping survey reveals that the most active elements like Cu and Ni were uniformly distributed throughout the sample. ICP-OES was used to determine the percentage ratio of Cu and Ni in 5 wt% of (1 : 1) Cu(0)–Ni(0)–AAPTMS@GO catalyst and it was found to be Cu/Ni ratio 0.98 *i.e.*, Cu is slightly lower loading than Ni. This may be

Fig. 4 SEM image of (a) AAPTMS@GO (b) Cu–AAPTMS@GO (c) (1 : 1) Cu–Ni–AAPTMS@GO (d) (1 : 1) Cu(0)–Ni(0)–AAPTMS@GO (e) (1 : 2) Cu(0)–Ni(0)–AAPTMS@GO and (f) (2 : 1) Cu(0)–Ni(0)–AAPTMS@GO.

due to Ni, more electronegative than Cu, which can more easily coordinate to the electron donating N atom of AAPTMS group present on the amine functionalized graphene oxide surface.

HRTEM was also used to further investigate the morphologies, diffraction pattern and lattice fringes of the materials. The different magnification of (1 : 1) Cu(0)–Ni(0)–AAPTMS@GO material with spherical nano particles can be seen in Fig. 6(a)–(e). From Fig. 6(g) showing the SAED pattern of the polycrystalline diffraction rings, (111) and (200) planes were indexed as the brighter inner diffraction ring and dimmer outer ring. The lattice fringe presented in Fig. 6(f) shows the single crystalline nature of the bimetallic alloy nano particles with characteristic d-spacings of 0.20 nm for (111) planes of both Ni and Cu. Therefore, it was confirmed that the solid solution constitutes both Cu and Ni.

The TEM and HRTEM images of mono dispersed bimetallic nano particles with histogram of particle size distribution plot for the Cu–Ni nanoparticles are shown in the [Fig. 7(a) and (b)]. From this Fig. 7, the average diameter of particle size is calculated to be ~4 nm with a narrow size variation.

3.2 Hydrogenation of unsaturated aldehydes

The scope of these novel nanomaterials was investigated on hydrogenation of unsaturated aldehyde to form an unsaturated alcohol product. Initially, to compare the activity and choice of different metal and different ratio of bimetallic modified functionalized GO were screened and the results are presented in the Table 1. A perusal of results in Table 1 shows that (1 : 1) Cu(0)–Ni(0)–AAPTMS@GO nano materials gave excellent results compare to mono metallic and other bimetallic catalysts, due to
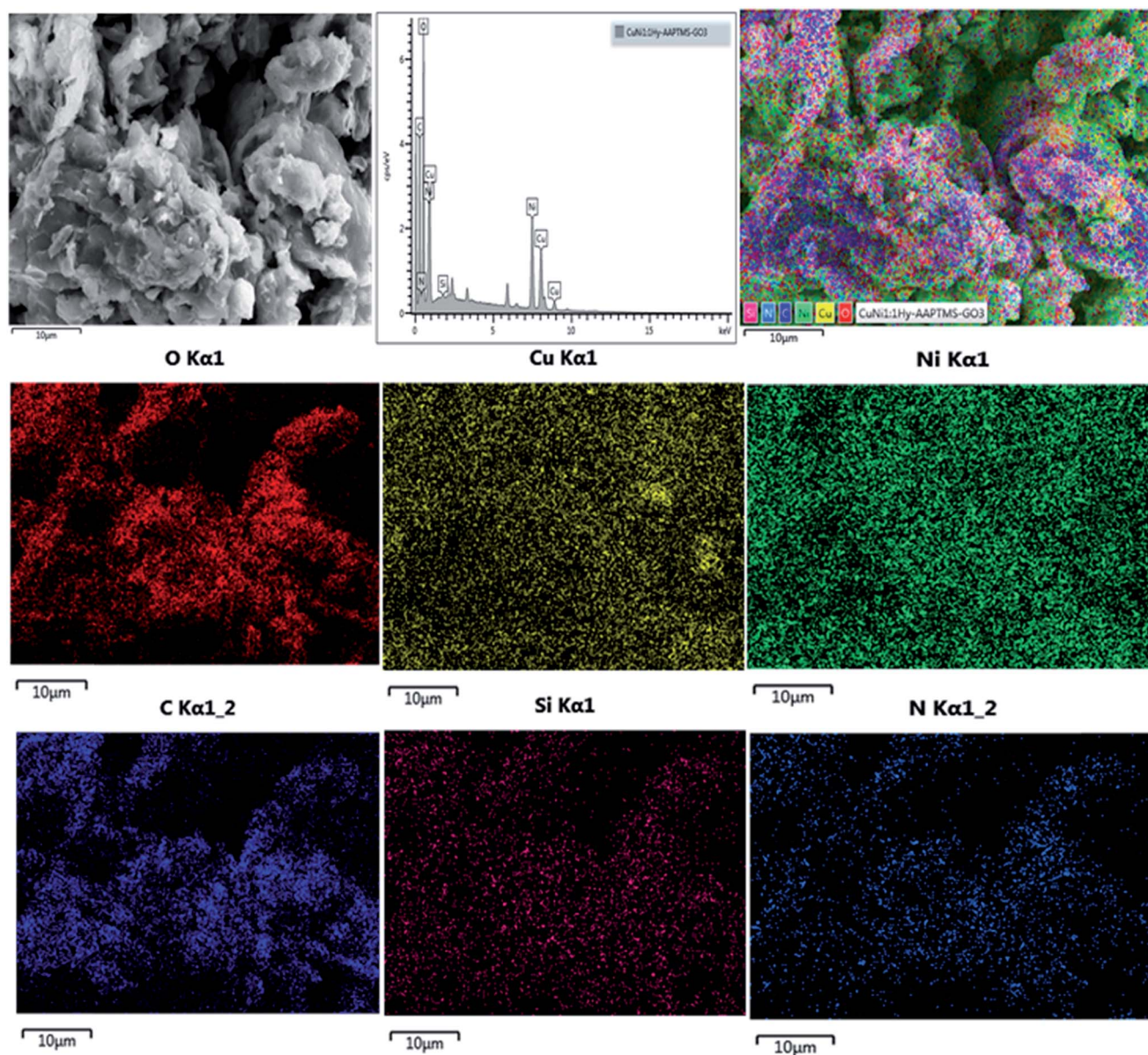

Fig. 5   SEM/EDX (scale bar = 10 μm) mapping of (1 : 1) Cu(0)–Ni(0)–AAPTMS@GO sample.

synergetic effect and uniform distribution as well as sufficient amount of metal particles. In case of (1 : 2) and (2 : 1) wt% composites, *i.e.*, with one metal in excess than other, and their activity was lower for same reaction. That excess presence of one metal causes imbalance in the even distribution of active sites of the metals on the catalyst surface for the hydrogenation of unsaturated aldehyde. Hence, the activity of the catalyst decreased. With increase in the temperature (90–120 °C), the conversion of unsaturated aldehyde increased from 85% up to 98% and but selectivity towards cinnamyl alcohol (COL) decreased significantly (Table 2). This may be due to weakly adsorbed hydrogen on the catalyst surface, which enhances the conversion of COL to hydrocinnamyl alcohol (HCOL) at higher rate. Hence, the selectivity to cinnamyl alcohol decreases with rise in temperature.

Table 3 presents the activity/selectivity of hydrogenation of unsaturated aldehyde by (1 : 1) Cu(0)–Ni(0)–AAPTMS@GO nano materials under same reaction conditions, but in different solvent media, such as water, methanol and isopropyl alcohol. The hydrogenation reaction with methanol as solvent gave better conversion and selectivity towards COL compared to

other solvents. This could be due to higher dipole moment as well as higher solubility of hydrogen in methanol.

3.3 Reduction of *p*-nitrophenol

Liu *et al.*[34] have reported the reduction of *p*-nitro phenol to *p*-aminophenol with 99% conversion at 100 °C. Motoyama *et al.*,[35] have reported >99% selectivity of nitro group reduction after 4 h reaction time. Various reports for reduction of PNP to PAP with varied conversions are also available in the literature which used metal nanoparticle systems,[36–43] Ni/SiO$_2$–AlO$_3$ (ref. 44) and Pd/Cu, Pt/Cu, Pt/Au, Pd/Au and Au/Cu dendrimer encapsulated nanoparticles[45] as catalysts. The *p*-nitrophenol to *p*-amino-phenol by NaBH$_4$, Pd/rGO proved better catalyst than the commercial Pd/C as reported by Sun *et al.*[46] Göksu *et al.*,[47] reported that hydrogenation of nitro/nitrile compounds with ammonia/borane catalysed by NiPd/GO nanoparticles gave ≥99% yield in presence of water and methanol within (5–30 min) at room temperature. A Pd/Cu nanoparticle supported on graphene gives 98% yield with 1.5 h reported by Xu *et al.*[1]

In the current study the broader utility of Cu–Ni bimetallic graphene oxide nanocomposites as catalysts for hydrogenation

Fig. 6 HRTEM image of different magnification of (a–e) (1 : 1) Cu(0)–Ni(0)–AAPTMS@GO (f) lattice fringes of (1 : 1) Cu(0)–Ni(0)–AAPTMS@GO (g) SAED pattern of (1 : 1) Cu(0)–Ni(0)–AAPTMS@GO.

Fig. 7 (a) TEM (scale bar = 100 nm) and (b) HRTEM (scale bar = 50 nm) image at high magnification with particle size distribution plot of the (1 : 1) Cu(0)–Ni(0)–AAPTMS@GO.

of nitro phenol was investigated with NaBH$_4$ as hydrogen source and water as solvent. The (1 : 1) Cu(0)–Ni(0)–AAPTMS@GO as catalyst gave highly impressive results with 100% conversion and selectivity towards *p*-amino phenol and reaction finished in 16 min at RT, while the 1 : 2 and 2 : 1 compositions recorded lower selectivity and conversions. These results prove superior to the literature reported results in terms of both conversion and selectivity efficiency and reaction conditions and time needed.

The hydrogen abstraction from BH$_4$⁻ and transferring to *p*-nitrophenolate anion occurred efficiently by the bimetallic alloy particles on the amino functionalised graphene oxide surface. The reduction of aromatic nitro compound was monitored by UV-Vis study. In UV-Vis, the peak at 400 nm indicates *p*-nitro-phenolate anion and at 300 nm indicates the product of *p*-aminophenol with (1 : 1) Cu(0)–Ni(0)–AAPTMS@GO catalyst shown in ESI Fig. S3.† In Fig. S3(A),† shows the decrease in

absorbance at 400 nm, due to the consumption of *p*-nitro-phenolate anion intermediate and the increase of intensity at 300 nm due to the formation of product, *p*-aminophenol. The representative products were characterized by ¹H NMR, ¹³C NMR and FTIR spectroscopies for conformational study in ESI Fig. S4(a–c).† (1 : 1) Cu–Ni–AAPTMS@GO catalyst showed very less activity due to the presence of different form of metallic phases, which was confirmed from the XRD results. However, the (1 : 1) Cu(0)–Ni(0)–AAPTMS@GO catalyst displayed the best catalytic activity towards *p*-amino phenol reduction, when compared to (1 : 2) Cu(0)–Ni(0)–AAPTMS@GO and (2 : 1) Cu(0)–Ni(0)–AAPTMS@GO. The high activity of (1 : 1) Cu(0)–Ni(0)–AAPTMS@GO was due to good dispersion of the (1 : 1) ratio of Cu–Ni bimetallic alloy nanoparticles on the functionalized graphene oxide sheets and the enhanced adsorption ability of graphene oxide for *p*-nitrophenol stems from the π–π stacking interactions. From Fig. S3(B) and (C),† it can be deduced that

Table 1 Conversion and selectivity data for hydrogenation with different metal loaded functionalized catalysts[a]

Catalyst	Conv. (%)	Product selectivity (%)			
		HCAL	COL	HCOL	Others
Cu–AAPTMS@GO	39	26.5	30.0	42.4	1.1
Ni–AAPTMS@GO	44	26.2	32.7	40.3	0.8
(1 : 1) Cu–Ni–AAPTMS@GO	52	18	42.2	38.5	1.3
(1 : 1) Cu(0)–Ni(0)–AAPTMS@GO	85	17.6	59.8	22.4	0.2
(1 : 2) Cu(0)–Ni(0)–AAPTMS@GO	82	11.8	51.3	36.3	0.6
(2 : 1) Cu(0)–Ni(0)–AAPTMS@GO	79	14.4	49.0	35.7	0.9

[a] Catalyst (150 mg), cinnamaldehyde (1.2 g), methanol (16 ml), time (1 h), and temp. (80 °C).

Table 2 Conversion and selectivity data at different temperature by (1 : 1) Cu(0)–Ni(0)–AAPTMS@GO catalyst[a]

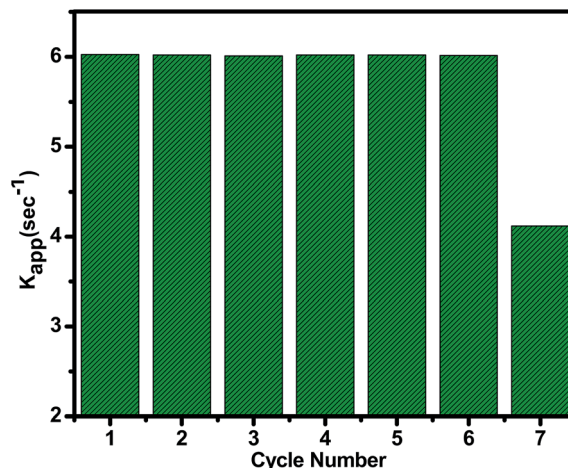| Temperature	Conv. (%)	Product selectivity (%)			
		HCAL	COL	HCOL	Others
90 °C	89	14.9	50.8	33.8	0.5
100 °C	92	12.3	42	44.5	1.2
120 °C	98	10.4	21.5	66.7	1.4

[a] Catalyst (150 mg), cinnamaldehyde (1.2 g), methanol (16 ml), time (1 h), and temp. (90–120 °C).

the reduction of nitro compound to amino compound over (1 : 1) Cu(0)–Ni(0)–AAPTMS@GO follow pseudo first-order kinetics for the chosen conditions.

Best features of ideal heterogeneous catalyst are high selectivity, high activity, long lifetime and cost effectiveness. The recyclability of the heterogeneous catalyst is vital parameter and it depends on its stability and the easy separability. The activity can change due to leaching of some metal particles into the reaction medium or may be the coke formation on the catalyst surface in the high temperature reactions. To test its robustness, the recovered catalyst was reused after regeneration followed by wash with water and calcination. No noticeable change up to 6th cycle was observed with activity remaining intact (Fig. 8). The catalyst did not leach out in this medium showing strong interaction between nanoparticles and amino group. The decrease in 7th circle could be due to some leaching Cu metal as compared to Ni. The binding capacity of Ni is higher than Cu, which can be more easily coordinated to the electron donating N atom of organic group present on the amine functionalized graphene oxide surface. The catalytic activity of hydrogenation of unsaturated aldehyde gives good conversion and selectivity and also the catalyst activity decreased (8%) in 5th cycle.

The reduction of PNP to PAP performance of (1 : 1) Cu(0)–Ni(0)–AAPTMS@GO was evaluated and compared with the state of the art in the corresponding field in Table 4. The Pd/C and Pd/G catalysts[46] the activity decreased in every cycle reaching 85% in the 5th cycle. With CuFe$_2$O$_4$ MNPs catalyst[50] catalyst was stable up to 2nd cycles only. So, that our (1 : 1) Cu(0)–Ni(0)–AAPTMS@GO catalyst has better recyclability and reusability.

The XRD, FTIR, SEM, TEM, HRTEM analysis of sixth cycle of reused catalyst are shown in ESI Fig. S5.† In the XRD spectra of reused (1 : 1) Cu(0)–Ni(0)–AAPTMS@GO catalyst, the strong and

Table 3 Conversion and selectivity data in presence of different solvents at 80 °C by (1 : 1) Cu(0)–Ni(0)–AAPTMS@GO catalyst[a]

Solvent	Conv. (%)	Product selectivity (%)			
		HCAL	COL	HCOL	Others
Methanol	85	17.6	59.8	22.4	0.2
Isopropyl alcohol	62	22.6	51.1	25.6	0.7
Water	57	45	21.8	32.8	0.4

[a] Catalyst (150 mg), cinnamaldehyde (1.2 g), time (1 h), and temp. (80 °C).

Fig. 8 The catalytic performance within seven cycles for the reduction of p-nitro phenol catalyzed by (1 : 1) Cu(0)–Ni(0)–AAPTMS@GO catalyst.

Table 4 Comparison of the catalytic reduction of nitrophenol compounds using various catalysts

Materials	Rate constant	Cycle	Ref.
p(AMPS)–Co composite	0.12 min^{-1}	5	48
Ag/CA	1.03–1.04 × 10^{-3} M min^{-1}	3	49
CuFe$_2$O$_4$ MNPs	7.2 min^{-1}	2	50
Pd/GO	0.0365 s^{-1}	1–5	46
Pd/C	0.0155 s^{-1}	1–5	46
(1 : 1) Cu(0)–Ni(0)–AAPTMS@GO	6.018 s^{-1}	6	Our work

active diffraction peak of nano particle at $2\theta = 43.51°$ for (111) plane, disappeared in the 7th cycle, although it can be seen after recycling it for the 6th cycle catalyst [Fig. S5(a) and (b)†]. From FTIR also it can be seen that the stretching vibrations of Si–O–C peak vanished after 6th cycle in [Fig. S5 (c) and (d)†]. The SEM, TEM and HRTEM images [Fig. S5(e)–(g)†] of the 6th cycle reused catalyst show no obvious change in morphology of the nanoparticles i.e., well-dispersed nanoparticles as like the fresh sample. Agglomerated bimetallic Cu–Ni nano particles were observed in the SEM, TEM and HRTEM images [Fig. S5(h)–(j)†] of the (1 : 1) Cu(0)–Ni(0)–AAPTMS@GO catalyst reused after six times.

4 Conclusions

In conclusion, in an environmentally friendly route different ratios of bimetallic Cu–Ni nanoparticles supported on organic functionalized graphene oxide were effectively prepared with an average particle size of 4 nm by a simple procedure. The 1 : 1 ratio of the nano catalyst was found to be highly efficient (100% conversion and selectivity in <20 min at RT) and reusable and towards reduction of nitro compounds with water as solvent. The same proved ideal for hydrogenation of cinnamaldehyde

with good conversion and selectivity with methanol as solvent. The activity was due to synergistic interactions between two metals involving charge transfer from one metal to another metal to form a Cu–Ni hetero structures with specific geometry in addition to the amino functionalized GO surface. The formation of bimetallic Cu–Ni particles was confirmed from XRD and XPS studies. From FT-IR and TEM analysis, covalent binding of the organic group of AAPTMS onto graphene oxide layer was confirmed. TEM and HR-TEM also confirmed that bimetallic Cu–Ni nanoparticles were uniformly distributed on the functionalized graphene oxide surface. The recovered catalyst can be recycled after activation. Bimetallic materials show higher CAL conversion and selectivity towards COL at lower temperatures, 80 °C and at higher temperatures (90–120 °C), while the conversion of CAL increased, selectivity towards COL got decreased due to weak adsorption of hydrogen on bimetallic catalysts surface at those temperatures.

Acknowledgements

References

1 Y.-S. Feng, J.-J. Ma, Y.-M. Kang and H.-J. Xu, *Tetrahedron*, 2014, **70**, 6100–6105.

2 Y. Veena, G. Shweta, K. Rupesh, S. Gajendra and L. Rekh, *Synth. Commun.*, 2012, **42**, 213–222.

3 J. Feng, J. M. Slocik, M. Sarikaya, R. R. Naik, B. L. Farmer and H. Heinz, *Small*, 2012, **8**(7), 1049–1059.

4 G. R. Rao, *Curr. Sci.*, 1998, **75**, 901–910.

5 T. Yamauchi, Y. Tsukahara, T. Sakata, H. Mori, T. Yanagida, T. Kawai and Y. Wada, *Nanoscale*, 2010, **2**, 515–523.

6 S. K. Singh, A. K. Singh, K. Aranishi and Q. Xu, *J. Am. Chem. Soc.*, 2011, **133**, 19638–19641.

7 N. V. Long, T. D. Hien, T. Asaka, M. Ohtaki and M. Nogami, *Int. J. Hydrogen Energy*, 2011, **36**, 8478–8491.

8 M. S. Wong, P. J. J. Alvarez, Y. Fang, N. Akçin, M. O. Nutt, J. T. Miller and K. N. Heck, *J. Chem. Technol. Biotechnol.*, 2009, **84**, 158–166.

9 (a) N. Dimitratos, J. A. Lopez-Sanchez and G. J. Hutchings, *Chem. Sci.*, 2012, **3**, 20–44; (b) S. E. Davis, M. S. Ide and R. J. Davis, *Green Chem.*, 2013, **15**, 17–45.

10 (a) C. George, A. Genovese, A. Casu, M. Prato, M. Povia, L. Manna and T. Montanari, *Nano Lett.*, 2013, **13**, 752–757; (b) J. Xu, T. White, P. Li, C. He, J. Yu, W. Yuan and Y.-F. Han, *J. Am. Chem. Soc.*, 2010, **132**, 10398–10406.

11 N. Dimitratos, A. Villa, D. Wang, F. Porta, D. Su and L. Prati, *J. Catal.*, 2006, **244**, 113–121.

12 J. K. Edwards, S. J. Freakley, A. F. Carley, C. J. Kiely and G. J. Hutchings, *Acc. Chem. Res.*, 2014, **47**, 845–854.

13 L. Kesavan, R. Tiruvalam, M. H. A. Rahim, M. I. bin Saiman, D. I. Enache, R. L. Jenkins, N. Dimitratos, J. A. Lopez-

Sanchez, S. H. Taylor, D. W. Knight, C. J. Kiely and G. J. Hutchings, *Science*, 2011, **331**, 195–199.

14 (a) D. Martin Alonso, S. G. Wettsteina and J. A. Dumesic, *Chem. Soc. Rev.*, 2012, **41**, 8075–8098; (b) H. Zhanga and N. Toshima, *Catal. Sci. Technol.*, 2013, **3**, 268–278.

15 V. K. Gupta, I. Tyagi, H. Sadegh, R. S. Ghoshekandi, A. S. H. Makhlouf and B. Maazinejad, *Sci. Technol. Dev.*, 2015, **34**, 195–214.

16 V. K. Gupta, R. Kumar, A. Nayak, T. A. Saleh and M. A. Barakat, *Adv. Colloid Interface Sci.*, 2013, **193–194**, 24–34.

17 V. K. Gupta, S. Agarwal and T. A. Saleh, *J. Hazard. Mater.*, 2011, **185**, 17–23.

18 T. A. Saleh and V. K. Gupta, *Adv. Colloid Interface Sci.*, 2014, **211**, 93–101.

19 A. K. Geim and K. S. Novoselov, *Nat. Mater.*, 2007, **6**, 183–191.

20 G. B. B. Varadwaj and V. O. Nyamori, *Nano Res.*, 2016, **9**, 3598–3621.

21 L. Yang, S. Luo, Y. Li, Y. Xiao, Q. Kang and Q. Cai, *Environ. Sci. Technol.*, 2010, **44**, 7641–7646.

22 M. G. Prakash, R. Mahalakshmy, K. R. Krishnamurthy and B. Viswanathan, *Catal. Today*, 2016, **263**, 105–111.

23 W. Lin, H. Chang, L. He, Y. Yu and F. Zhang, *J. Catal.*, 2013, **303**, 110–116.

24 G. X. Zhao, X. M. Ren, X. Gao, X. L. Tan, J. X. Li, C. L. Chen, Y. Y. Huang and X. K. Wang, *Dalton Trans.*, 2011, **40**, 10945–10952.

25 Y. J. Li, W. Gao, L. J. Ci, C. M. Wang and P. M. Ajayan, *Carbon*, 2010, **48**, 1124–1130.

26 H. K. Jeong, Y. P. Lee, R. J. W. E. Lahaye, M. H. Park, K. H. An, I. J. Kim, C.-W. Yang, C. Y. Park, R. S. Ruoff and Y. H. Lee, *J. Am. Chem. Soc.*, 2008, **130**, 1362–1366.

27 J. J. Niu and J. N. Wang, *Electrochim. Acta*, 2008, **53**, 8058–8068.

28 S. Rana, S. Maddila and S. B. Jonnalagadda, *Catal. Sci. Technol.*, 2015, **5**, 3235–3241.

29 N. H. Kim, T. Kuila and J. H. Lee, *J. Mater. Chem. A*, 2013, **1**, 1349–1358.

30 G. MO, W.-D. Cheng, Q. Cai, W. Wang, K.-H. Zhang, X.-Q. Xing, Z.-J. Chen and Z.-H. Wu, *Mater. Chem. Phys.*, 2010, **121**, 390–394.

31 S. Rana, S. Maddila, K. Yalagala and S. B. Jonnalagadda, *Appl. Catal., A*, 2015, **505**, 539–547.

32 Q. Zhao, Y. Li, R. Liu, A. Chen, G. Zhang, F. Zhang and X. Fan, *J. Mater. Chem. A*, 2013, **1**, 15039–15045.

33 *Handbook of X-ray Photoelectron Spectroscopy*, Physical Electronic Division, Perkin-Elmer, 1979, vol. 55, p. 344.

34 H. Liu, J. Deng and W. Li, *Catal. Lett.*, 2010, **137**, 261–266.

35 M. Takasaki, Y. Motoyama, K. Higashi, S. Yoon, I. Mochida and H. Nagashima, *Org. Lett.*, 2008, **10**, 1601–1604.

36 S. K. Ghosh, M. Mandal, S. Kundu, S. Nath and T. Pal, *Appl. Catal., A*, 2004, **4**, 61–66.

37 S. Wunder, Y. Lu, M. Albrecht and M. Ballauff, *ACS Catal.*, 2011, **1**, 908–916.

38 I. H. A. E. Maksod, E. Z. Hegazy, S. H. Kenawy and T. S. Saleh, *Adv. Synth. Catal.*, 2010, **352**, 1169–1178.

39 S. Jana, S. K. Ghosh, S. Nath, S. Pande, S. Praharaj, S. Panigrahi, S. Basu, T. Endo and T. Pal, *Appl. Catal., A*, 2006, **313**, 41–48.

40 X. Bai, Y. Gao, H. Liu and L. Zheng, *J. Phys. Chem. C*, 2009, **113**, 17730–17736.

41 Z. V. Feng, J. L. Lyon, J. S. Croley, R. M. Crooks, D. A. V. Bout and K. J. Stevenson, *J. Chem. Educ.*, 2009, **86**, 368–372.

42 S. Sarkar, M. Pradhan, A. K. Sinha, M. Basu, Y. Negishi and T. Pal, *Inorg. Chem.*, 2010, **49**, 8813–8827.

43 S. Wunder, F. Polzer, Y. Lu, Y. Mei and M. Ballauff, *J. Phys. Chem. C*, 2010, **114**, 8814–8820.

44 M. A. Cangiano, M. W. Ojeda, A. C. Carreras, J. A. González and M. C. Ruiz, *Mater. Charact.*, 2010, **61**, 1135–1146.

45 Z. D. Pozun, S. E. Rodenbusch, E. Keller, K. Tran, W. Tang, K. J. Stevenson and G. Henkelman, *J. Phys. Chem. C*, 2013, **117**, 7598–7604.

46 J. Sun, Y. Fu, G. He, X. Sun and X. Wang, *Catal. Sci. Technol.*, 2014, **4**, 1742–1748.

47 H. Göksu, S. F. Ho, O. Metin, K. Korkmaz, A. M. Garcia, M. S. Gültekin and S. Sun, *ACS Catal.*, 2014, **4**, 1777–1782.

48 N. Sahiner, H. Ozay, O. Ozay and N. Aktas, *Appl. Catal., B*, 2010, **101**, 137–143.

49 S. Saha, A. Pal, S. Kundu, S. Basu and T. Pal, *Langmuir*, 2010, **26**, 2885–2893.

50 J. Feng, L. Su, Y. Ma, C. Ren, Q. Guo and X. Chen, *Chem. Eng. J.*, 2013, **221**, 16–24.